A NOVEL INITIAL ORBIT DETERMINATION ALGORITHM FROM DOPPLER AND ANGULAR OBSERVATIONS

C. Yanez, F. Mercier, and J-C. Dolado

CNES, 18 av. Edouard Belin, 31401 Toulouse Cedex 9, France, Email : carlos.yanez@cnes.fr

ABSTRACT

A novel numerical method for solving the initial orbit determination (IOD) problem is developed in the frame of space debris surveillance systems. Differently from classical IOD methods, where three sets of angles or two position vectors are used, the method presented in this paper makes use of N Doppler measurements along with their associated pairs of angular measurements coming from an Earth-based radar station. Numerical results are presented for objects in three different Low Earth Orbits (LEO) showing the accuracy and performances obtained by this method.

Key words: Initial Orbit Determination; Doppler Radar; Space Debris; Cataloguing; LEO objects.

1. INTRODUCTION

Space Situational Awareness (SSA) refers to the ability to view, understand and predict the physical location of natural and manmade objects in orbit around the Earth. While the ability to view is made possible thanks to ground and space based sensors (e.g. Radars, Telescopes or Lasers), the ability to understand and predict the physical location of objects needs the determination of their orbital state vectors, which uniquely determine the trajectory of the object in space.

For the determination of the orbital state of an object, mainly two different situations have to be considered. Either the object is already catalogued (i.e. it is regularly observed by sensors and an a priori state vector is available) or the object has been newly discovered by a so-called surveillance sensor. In the first case, the *a priori* orbital state of the object can be refined thanks to the new gathered observations following a Least-Squares (LS) or an Extended Kalman Filter (EKF) filtering approach. In the second case, an *a priori* orbital state has to be computed from the gathered observations, in order to predict the position of the newly detected object at short term and to improve the accuracy of the orbit with the acquisition of new observations from surveillance and/or tracking sensors.

Present work is focused on the second problem, and, in particular, we develop a method to estimate an initial orbit from surveillance radar measurements. A distinctive feature of such surveillance radars is that they are, for the most part, Doppler radars, which means that they provide the angular measurements and the Doppler shift (i.e. the radial velocity) of the observed target at each observing time. While an extensive literature exists on algorithms to estimate an initial orbit from three pairs of angular measurements ([1], [2], [3]) or from two pairs of angular measurement and ranges (i.e., the Lambert's problem, [4], [5], [6]), few literature exist on methods to estimate an initial orbit from measurements coming from a Doppler radar.

On this paper we introduce the developed method, its practical implementation and its performance by means of several test scenarios with simulated data of LEO objects.

2. DESCRIPTION OF DOPPLER IOD ALGORITHM

In order to process surveillance radar data, it is necessary to be able to solve the initial orbit determination problem based on its measurements. Contrary to a tracking radar for which an *a priori* orbit is available, surveillance radar can produce measurements from non-catalogued objects.

It is assumed, then, that no information on the state-vector of the object is available. Radar data comprises N consecutive observations (gathered in an observation *arc* or observation *pass*), not necessary equally time spaced. Each observation is composed of measurements on the line of sight $\overline{L}$, defined by a pair of angles (for example, the right ascension α and the declination δ), and the Doppler shift $\dot{d}$ of the unknown object, where d is a distance that depends on the type of radar[1] and the dot represents the time derivative. In the case of a monostatic radar, this distance refers directly to the object

[1] We consider the cases of monostatic and bistatic radars. The former refers to a radar in which the transmitter and receiver are collocated, and the latter to a radar in which the transmitter and receiver are in different locations, maybe hundreds of km away.

Proc. 7th European Conference on Space Debris, Darmstadt, Germany, 18–21 April 2017, published by the ESA Space Debris Office
Ed. T. Flohrer & F. Schmitz, (http://spacedebris2017.sdo.esoc.esa.int, June 2017)

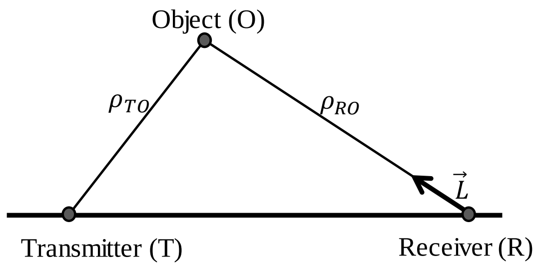

Figure 1: Scheme of the geometry for a bistatic sensor.

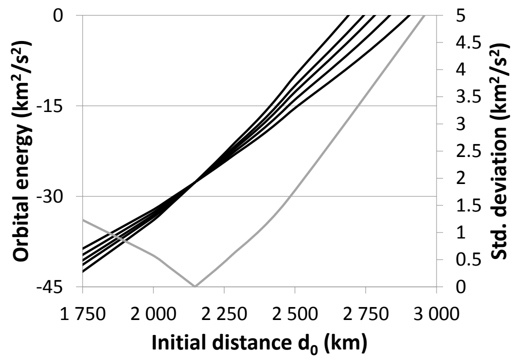

Figure 2: Specific orbital energy of the orbit passing through diffferent pairs of measurmeents as a function of the integration constant (black lines, left scale). Standard deviation of the distribution of energies (grey line, right scale). More pairs than those plotted are used in the computation of σ.

range, $d_{monostatic} = \rho$. This equation assumes implicitly that the propagation time in the two-way trip from ground-based radar to orbiting object is negligible and, in consequence, the epoch of emission and reception is the same (see Appendix to take into account this term). On the other hand, for bistatic radars, this distance corresponds to the transmitter-object-receiver distance, $d_{bistatic} = \rho_{TO} + \rho_{RO}$ (see Figure 1). In this case, we will speak of object range to the distance between the receiver and the object, which can be expressed as follows:

$$\rho = \frac{d^2 - |\overline{TR}|^2}{2(|\overline{TR}| \cdot \overline{L} + d)} \tag{1}$$

The estimation of the derived distance measurements $d(t)$ is the main concern of the algorithm, so that the Doppler initial orbit determination can be reduced to a well-known Lambert's problem between the boundaries of the observation arc. This estimation is performed using optimization techniques. We begin by integrating[2] the Doppler measurements between the initial time of the observation arc t_0 and a time $t \leq t_f$, where t_f is the final time of the observation arc:

$$d(t) = d_0 + \int_{t_0}^{t} \dot{d}\, dt. \tag{2}$$

This equation assumes that the radar is taken measurements of the object continuously within a visibility pass. For LEO objects, this visibility pass covers typically a few minutes span. The evolution in time of the distance d and, consequently, the evolution in time of the object range, is known up to a constant of integration d_0, which corresponds to the distance at the initial time. Somehow we are transforming the Doppler radar problem into a distance radar problem where an unknown bias on the distance measurement applies.

The procedure for the determination of this constant is based on the conservation, to first order, of the total orbital energy. Actually, the energy of the orbit that passes through any two observations can be determined as a function of d_0 by solving the associated Lambert's problem. Let $\overline{\rho}_i = \rho(t_i, d_0)\overline{L}_i$ and $\overline{\rho}_j$ be the position vectors of the selected pair of points (i, j) and $\Delta t = t_j - t_i > 0$ the corresponding flight time, we can then solve the Lambert's problem to get the specific orbital energy of the two-body problem, that is to say, $\epsilon_{ij}(d_0) = -\mu/2a$. An ideal two-body system is conservative, that is to say, the total energy of the problem is conserved. Furthermore, if we consider ideal (error-free) measurements, the curves $\epsilon_{ij}(d_0)$ for any combination of two observations intersect into a single point (see Figure 2). Thus, this point defines the initial range d_0 and, by extension, a preliminary estimate of the orbit. This point satisfies the energy integral of Kepler's motion and it is, in this way, the optimal solution. In a real case, however, the object will be subject to dissipative forces (for LEO objects, the atmospheric drag is the most important one), and the measurements will not be error-free but the sensor noise and bias should be considered. In this situation, a unique intersection in the graph $\epsilon(d_0)$ is not possible but, on the contrary, a distribution of energies ϵ_{ij} can be computed for any value of d_0. The value of d_0 that leads to the minimum standard deviation, σ_{min}, in the distribution of energies is the optimal solution. This distribution of energies depends directly on the way the pair of measurements (i,j) are selected. The selection cannot be done at random since observations needs to be handled equally (i. e. being selected the same number of times) in order not to introduce any artificial bias in the solution. In Section 3.1, different approaches are analysed.

Thus, the standard deviation of the distribution of energies is a univariate function that only depends on the integration constant, $\sigma(d_0)$. The minimization is performed by means of the Brent's method [8] that does not require the use of derivatives. The optimization search interval varies depending on the type of radar. For a monostatic radar we will search within the interval $[h_r/sin(el),\, \rho_{max}]$, where h_r is an altitude below which reentry is considered imminent ($\simeq$ 120 km), el is

[2] Within this work, numerical integration of the Doppler measurements is done through the Simpson's 3/8 rule, based upon a cubic interpolation. Equally spaced in time measurements are, in consequence, considered in the simulations.

Scenario	LEO_1	LEO_2	LEO_3
Semi-major axis [km]	7198.0	6778.0	7578.0
Eccentricity [-]	0.0	0.0	0.0
Inclination [deg]	98.71	60.00	60.00

Table 1: Keplerian orbital elements defining the three reference orbits.

Noise case	Angular noise σ_{ang} (mdeg)	Doppler noise σ_{dop} (cm/s)
Low noise	10.0	10.0
High noise	100.0	100.0

Table 2: Gaussian standard deviations of the measurements noise defining two noise cases.

the elevation and ρ_{max} the maximum range of radar acquisition. For a bistatic radar, this search interval stays $[2h_r/sin(\gamma),\ 2\rho_{max}]$, where $\gamma = atan(2h_r/|\overline{TR}|)$.

3. TEST SCENARIOS

Three reference orbits are selected as base scenarios for testing the developed method. These orbits are circular at altitudes of 400, 820 and 1200 km depending on the case. Additional numerical data defining the orbits considered are provided in Table 1. These scenarios only take into account LEO objects (altitude below 2000 km [7]), since the observation of objects orbiting on higher orbits is typically carried out with optical sensors. In all cases, the observations were made from a ground station located in France at the following geodetic coordinates: longitude = 7.0 deg, latitude = 44.0 deg and alt = 1200.0 m. Then, only monostatic radar results are presented in this paper. Nevertheless, same scenarios have been executed considering a bistatic radar (with a distance transmitter-receiver of 400 km), showing similar results. These three base scenarios are enriched by a sensitivity study concerning the following parameters:

- Measurement noise. In order to simulate realistic data, measurements are corrupted with a Gaussian noise characterized by its standard deviation σ. We consider angular noise σ_{ang}, equal in both directions (azimuth and elevation), going from 1 mdeg to 1 deg, and Doppler noise, σ_{dop} in the interval 1 cm/s to 10 m/s. Two main cases are usually reported as low and high noise case (see Table 2).

- Observation timespan ΔT. The duration of the observation interval has a direct impact on the accuracy of the orbit estimate since it is related to the observable portion of the orbit. We consider observation intervals up to 10 minutes for LEO_1 and LEO_3 scenarios that roughly corresponds to the first visibility interval, and up to 5 minutes for the LEO_2 scenario, which is the one at a lower altitude ($\simeq$ 400 km).

- Measurement acquisition frequency Δt. We consider time separation between observations that goes from 1 to 30 seconds. These measurements are taken all over the observation interval.

Results presented hereafter are all average values obtained from 1000 simulation runs.

3.1. Influence of the selection of measurements pairs

The aforementioned Doppler IOD method depends on the way the pair of measurements are selected to compute the distribution of energies. Two approaches are envisaged:

- Consecutive: We take one observation and the following one in such way as to have pairs of index covering the whole observation interval. We consider high frequency radar observations so that it is possible to compute the velocity with a finite differences approximation, $v_i = (r_{i+1} - r_i)/\Delta t$. We compute then the orbital energy as $\epsilon_{ij}(d_0) = v^2/2 - \mu/r$. We have made the assumption that close observations are not correlated to each other. In this work sensor noise is simulated with a Gaussian component added to the geometric value and, for each observation, the Gaussian noise is computed randomly, so independently of other observations.

- Half-arc separation: The idea behind this approach is to mitigate the effect of the measurement noise. Thus, we take measurements separated by a longer interval equal to the half of the observation interval (considering that observations are equally spaced in time). All the observations are considered once in the computation. Moreover, Izzo method [6] is used for solving the Lambert's problem instead of the simple finite differences scheme.

We have assessed both approaches with observations of the sun-synchronous case (LEO_1) covering a 10 mn timespan. It is worth noting that for close observations, the consecutive approach fails in providing a satisfactory orbit estimation (notice the error in semi-major axis shown in Figure 3). This behaviour can be explained by the influence of measurement noise on the Lambert's problem resolution when the observed portion of the orbit covers a tiny part (0.1% of the orbit for $\Delta t = 6$ s) and, in consequence, the relation $\Delta\alpha$, $\Delta\delta >> \sigma_{ang}$ between two measurements no longer stays. Half-arc separation approach presents, on the contrary, a more stable trend with respect to the time between measurements. We are solving in this case a Lambert's problem with bounds separated around 5 mn (all pairs are separated by

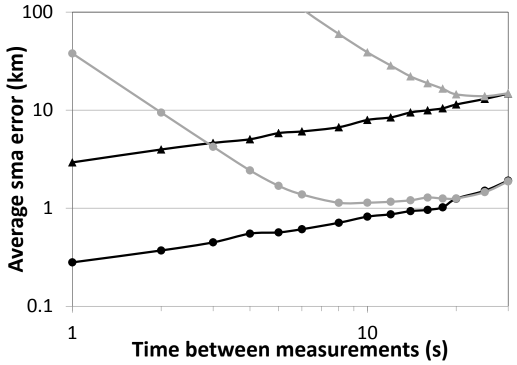

Figure 3: Average semi-major axis error for LEO_1 case with an observation timespan $\Delta T = 10\,mn$. Low noise case (circles) and high noise case (triangles) results are obtained either with half-arc separation (black) or consecutive approach (grey).

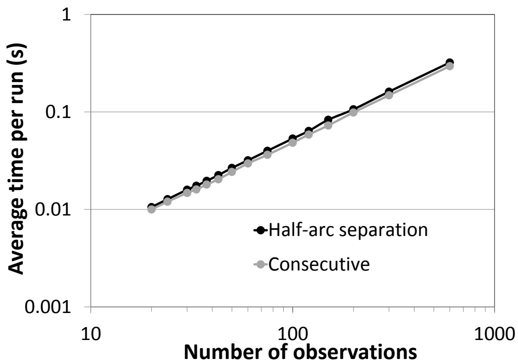

Figure 4: Average time per run in the LEO_1 case with an observation timespan $\Delta t = 10\,mn$.

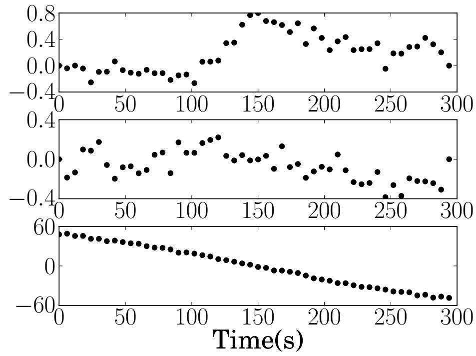

Figure 5: Residuals on azimuth [deg] (top), elevation [deg] (center) and radial velocity [m/s] (bottom) of a LEO_1 object with measurements corresponding to the high noise case taken within a $\Delta T = 5\,mn$.

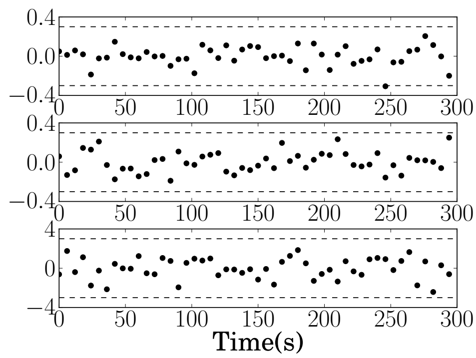

Figure 6: Residuals of Figure 5 when the initial orbit is refined with a least-squares filter. Dashed line corresponds to the values 3σ of the sensor noise.

the same timespan) which correspond to 5% of the orbit. For the half-arc separation approach, we identify two main elements having an impact on the orbit accuracy:

1. Measurement noise. We can see in Figure 3 that black lines are almost parallel. The difference between both lies in having increased the measurement noise in one order of magnitude in the three components observed (two angular values and Doppler). Accuracy in semi-major axis roughly decreases by one order of magnitude too.

2. Number of measurements. This is directly related to the quantity of information that is available about the orbit. When the observations pass from being spaced 1 s to 30 s in the same timespan, we are equivalently passing from 600 to only 20 observations. The less observations are available, the worse the distribution of energies is represented.

We have compared the computational time required by both approaches on a multi-core 2.66 GHz machine with 32 GB RAM. Results are plotted in Figure 4 showing a negligible difference between the approaches employed. We can thus state that the simple finite differences scheme does not speed up the computation significantly. Therefore, half-arc separation approach is selected as optimal in terms of accuracy and computational time. Results contained in the rest of this work refer invariably to this approach.

3.2. Scenario LEO_1 : sun-synchronous orbit

This scenario analyses the accuracy that can be obtained for an object in a sun-synchronous orbit at 820 km of altitude. If we look closely to the residuals that are obtained after applying the Doppler IOD method (see Figure 5), we notice that the estimates of the angular positions are roughly contained within the order of magnitude of the angular noise. However, estimates on the radial velocity present an important drift with respect to the observations. This fact indicates that the semi-major axis and eccentricity estimates are not as accurate as other angular-related elements as the inclination or the argument of lat-

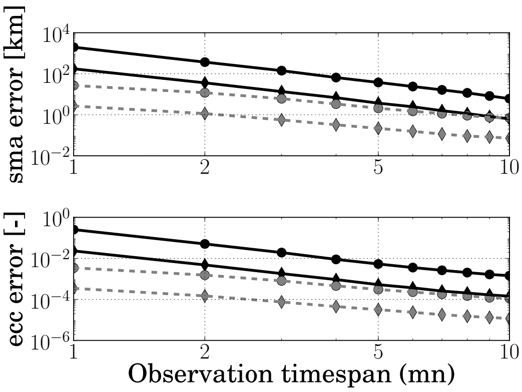

Figure 7: Average semi-major axis error [km] (top) and average eccentricity error (bottom) as a function of observation timespan ΔT. Circles correspond to the high noise case and diamonds to the low noise case. Solid black and dashed grey lines are the result of the Doppler IOD method before and after applying the LS filter, respectively. $\Delta t = 6$ s.

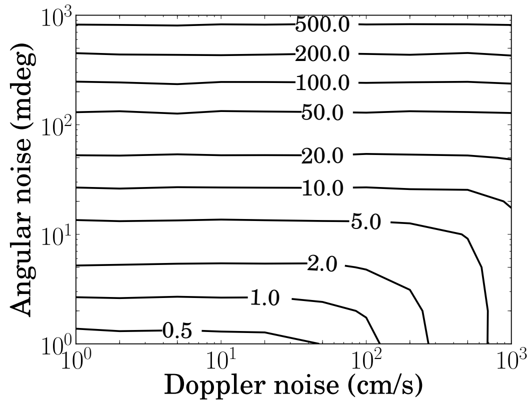

Figure 8: Average semi-major axis error [km] as a function of measurement noise. $\Delta T = 5\,mn$ and $\Delta t = 6\,s$.

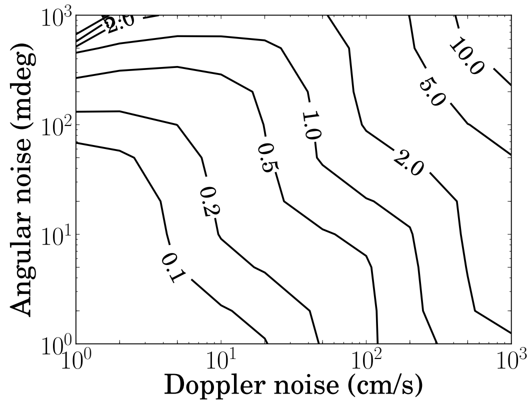

Figure 9: Average semi-major axis error [km] as a function of measurement noise after having refined the initial orbit with a LS filter. $\Delta T = 5\,mn$ and $\Delta t = 6\,s$.

itude. It is then necessary to refine the initial orbit by means of a least-squares filter in order to obtain an *optimal* orbit estimate. The effect of this LS step can be seen in Figure 6, where residuals in all three components of the observation stays within the band $\pm 3\sigma$. This optimal behaviour of the residuals in Figure 6 is attained by considering the same dynamical model in the simulated observation and in the LS filter. In a real case, the dynamical model used in the LS filter is essential to achieve comparable accuracies. For an object in the LEO regime, at least a dynamical model including osculating J2 effects is needed.

Sensitivity against the observation timespan can be seen in Figure 7. We highlight the constant trend observed in the accuracy obtained, which can be approximated to a power law. It is worth noting the remarkable improvement in the accuracy for longer timespans. This is due to a twofold reason. We are not only increasing the observed portion of orbit (with the consequently increase of knowledge about the shape of the orbit, i. e. the eccentricity), but we are at the same time increasing the number of observations, which helps in building up a more reliable distribution of energies, ϵ_{ij}, for the optimization problem.

Figure 8 plots the average semi-major error as a function of measurement noise. It is worth noting the preponderance of the angular noise over the Doppler one, shown up by the horizontal contour lines. For example, if the angular noise is above 30 mdeg, there is no difference if Doppler measurements are remarkable accurate with $\sigma_{dop} = 1$ cm/s or, on the contrary, are obtained with a less performant radar of 10 m/s noise. This behaviour changes after applying the LS filter and the contour plot exhibits, as expected, a diagonal increase of the error (towards the upper-right corner of the figure), that is to say, if the noise of any observational component increases, the accuracy obtained decreases. The orbital plane is, in general, well defined. The difficulty to both, recover the object a few orbital periods later and enable a LS filter to converge with a measurement arc containing several passes, comes essentially from the error in semi-major axis. It is worth thinking of in terms of orbital period. In this orbital regime, an error of 100 m in semi-major axis corresponds to a difference of about a tenth of second in a revolution, and in one day ($\simeq$ 14 revolutions) less than 2 s gap. Nevertheless, a 10 km error in semi-major axis is translated in a difference of $\pm$ 13 s in a revolution, and, in consequence, one day later the object will pass through the predicted region of sky about 3 minutes before or after the estimate, with a non-negligeable angular shift with respect to the line-of-sight prediction.

3.3. Scenarios LEO_2 and LEO_3 : low and high LEO objects

These two scenarios analyze the performance of the IOD Radar for objects at 400 and 1200 km of altitude, respectively. Figure 10 shows the sensitivity of the solution with

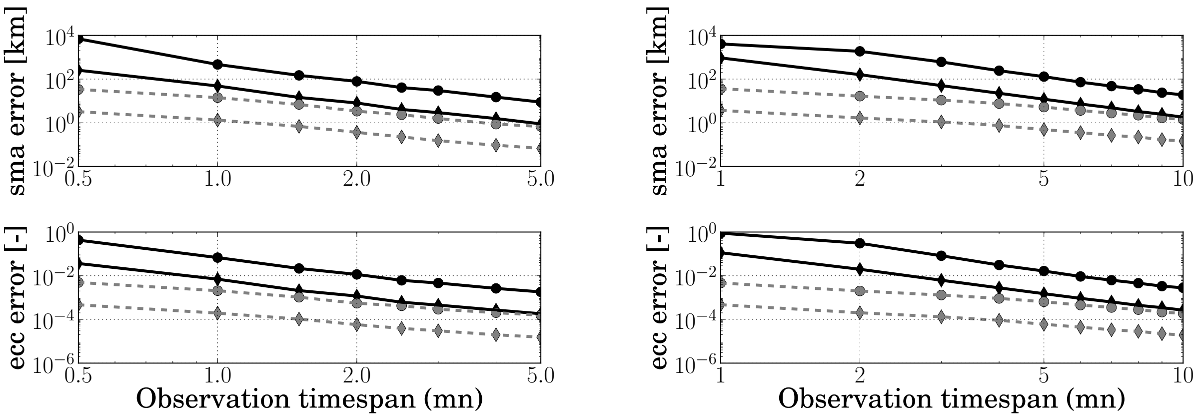

Figure 10: Average semi-major axis error [km] (top) and average eccentricity error (bottom) as a function of observation timespan ΔT, for LE0_2 (left) and LEO_3 (right) scenarios. See Figure 7 for more details on the legend.

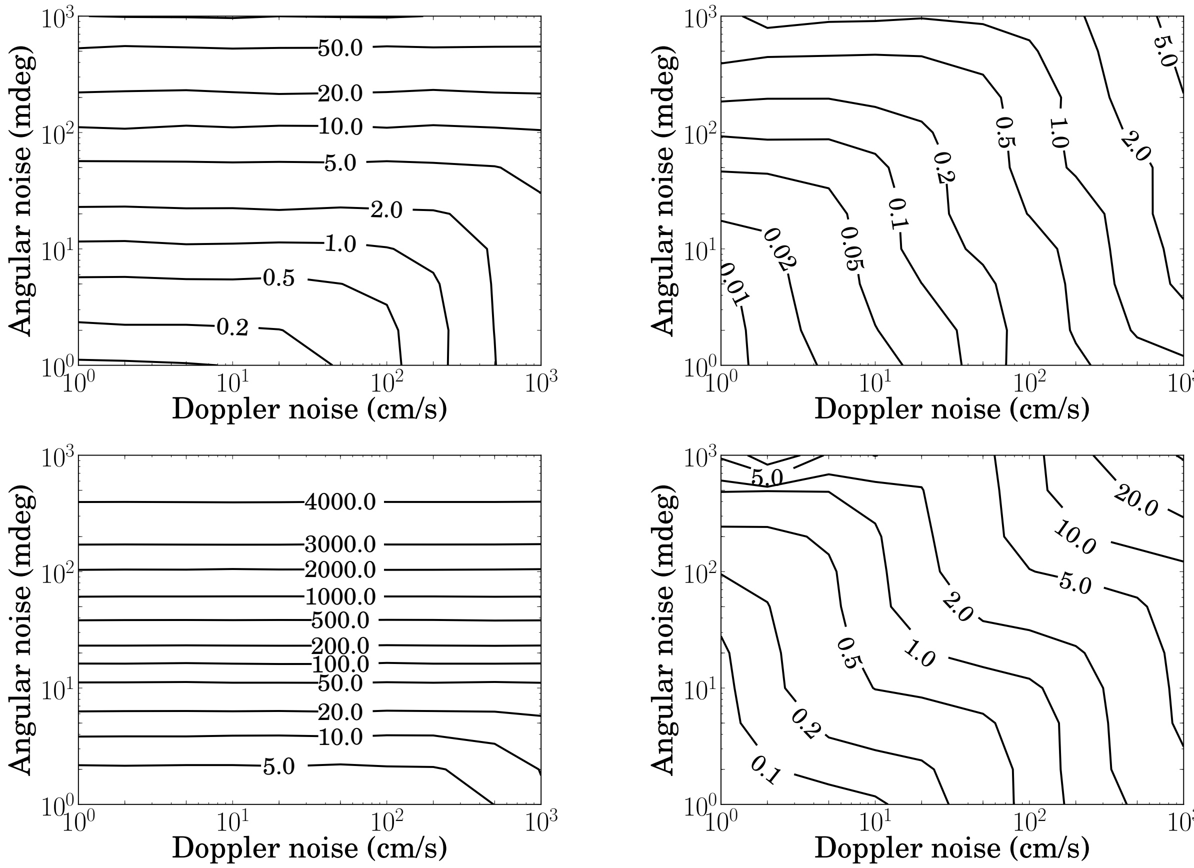

Figure 11: Average semi-major axis error [km] as a function of measurement noise. $\Delta T = 5\,mn$ and $\Delta t = 6\,s$. LEO_2 results are plotted at the top and LEO_3 results at the bottom. Results are presented before (left) and after (right) having refined the initial orbit with a LS filter.

respect to the observation timespan. Note that axes do not share the same scale, as visibility periods for the lower altitude case are limited to approximately 5 mn. In line with the results from previous section, we notice an outstanding improvement of the acccuracy obtained for longer timespans, in the form of a constant decreasing trend that can be fitted to a power law. It is important, then, to have access to a prolonged observation timespan that covers almost the entire visibility period. Comparing both scenarios, we observe that higher accuracies are obtained in the LEO_2 case, which is the one at a lower altitude. This fact is explained by two complementary reasons. First, the observable portion of the orbit decreases, for a fixed observation timespan, with the altitude of the object. For

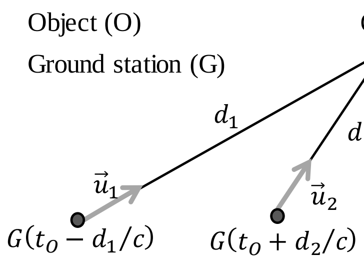

Figure 12: Scheme of time propagation effect on the geometry of the problem for a monostatic Doppler radar.

example, the percentage of observable orbit in 5 mn gets reduced from 5.4 to 4.6% as the altitude increases from 400 to 1200 km. The extension of the observable orbit arc limits the attainable accuracy. And second, the position error induced by the angular noise depends directly on the distance receiver-object, following the expression $\sigma_{pos} = \rho_{RO}\sigma_{ang}$.

We can see in Figure 11 the average semi-major error as a function of the measurement noise. We recover a similar behaviour than that of the previous section. The strength of the angular noise impact in the results is emphasized in the LEO_3 scenario (higher altitude), as expected. In that scenario, level curves are essentially horizontal, noting a minor influence of the Doppler noise on the orbit accuracy for the range of noise values explored. Again, the use of the LS filter is necessary to greatly reduce the error on the semi-major axis. In the configuration with the less performant radar, we obtain accuracies on the semi-major axis of the order of 5 and 20 km for LEO_2 and LEO_3 scenarios, respectively. If we repeat the exercise in terms of orbital periods, we have that, for the LEO_2 regime, an error of 5 km corresponds to a difference of ± 6 s in a revolution, and in one day ($\simeq$ 15.5 revolutions) around 1m30s gap. Furthermore, in the LEO_3 scenario, an error of 20 km in the semi-major axis induces a difference of ± 26 s in the orbital period. This causes, in one day (± 13 revolutions), an uncertainty of more than 5mn30s on the predicted moment for the radar to track the object again (considering an optimistic angular shift contained within the field of regard of the radar). Hence, the importance of re-observe the object in the early revolutions after its identification in order to achieve a good estimate on the semi-major axis, that permit us to consolidate the object orbit in the catalogue.

4. CONCLUSIONS

On this paper we have introduced a novel method to compute the initial orbit of an orbiting object in the LEO regime from Doppler radar measurements, including monostatic and bistatic radar types. It is composed of two steps. First step, an optimization problem is built up taking into account energetic considerations in order to reduce the problem to a two-body Lambert's problem. Second step, the initial orbit obtained previously is fitted to observations in a LS filter with a more complex dynamical model. The performance of this approach has been assessed by the definition and analysis of three synthetic cases including LEO object at different orbital regimes. Furthermore, the robustness of the algorithm to a variation on the quality and quantity of information has also been assessed, by a sensitivity analysis on the measurements noise, the observation timespan and the time between measurements. In addition, the accuracy of the proposed algorithm has been demonstrated through the different simulation scenarios, which highlight the efficiency of the algorithm to estimate an initial orbit from N observations coming from a Doppler radar.

APPENDIX : CONSIDERING PROPAGATION TIME

The propagation time of the two-way trip between a ground station and an object is modelled by the following equations:

$$d_1 = |D(t_D)G(t_D - d_1/c)|, \tag{3}$$
$$d_2 = |D(t_D)G(t_D + d_2/c)|, \tag{4}$$
$$d = (d_1 + d_2)/2, \tag{5}$$
$$\dot{d} = \texttt{Doppler measurement}, \tag{6}$$

where t_D is the date of signal reflection by the object, c is the speed of light and d_1 and d_2 are described in Figure 12. These equations shall be solved completely, with an iterative scheme, for the reception time at the beginning and end of the Doppler signal. A solver dedicated to this problem should be included in the LS filter step to take into account the effects of geometric propagation time. Similar equations can be derived for bistatic radars.

REFERENCES

1. Vallado D. A. (2007). *Fundamentals of astrodynamics and applications*. Third Edition. Microcosm, Hawthorne, CA.
2. Escobal P.R. (1965). *Methods of Orbit Determination*. John Wiley and Sons, Inc., New York
3. Gooding R. H. (1997). A new procedure for the solution of the classical problem of minimal orbit determination from three lines of sight, *Celest. Mech. Dyn. Astr.*, **66**(4), 387-423
4. Lancaster E. and Blanchard R. (1969). A unified form of Lambert's theorem. National Aeronautics and Space Administration. Technical Note D-5368.
5. Gooding R. H. (1990). A procedure for the solution of lambert's orbital boundary-value problem, *Celest. Mech. Dyn. Astr.*, **48**(2), 145-165
6. Izzo D. (2015). Revisiting Lamberts problem, *Celest. Mech. Dyn. Astr.*, **121**(1), 1-15

7. Inter-Agency Space Debris Coordination Committee (2007). IADC Space Debris Mitigation Guidelines, IADC-02-01

8. Brent R. P. (1973). *Algorithms for minimization without derivatives*. Prentice-Hall series in automatic computation.